Biosensors and Bioelectronics 194 (2021) 113604

Contents lists available at ScienceDirect

Biosensors and Bioelectronics

journal homepage: www.elsevier.com/locate/bios

A disposable, wearable, flexible, stitched textile electrochemical biosensing platform

Andrew Piper *, Ingrid Öberg Månsson, Shirin Khaliliazar, Roman Landin, Mahiar Max Hamedi **

Department of Fibre and Polymer Technology, KTH Royal Institute of Technology, Teknikringen 56, Stockholm, 10044, Sweden

ARTICLE INFO

Keywords:
Wearable
Textile
Disposable
Au-thiolate self-assembled monolayers
Glucose in sweat

ABSTRACT

Wearable sensors are a fast growing and exciting research area, the success of smart watches are a great example of the utility and demand for wearable sensing systems. The current state of the art routinely uses expensive and bulky equipment designed for long term use. There is a need for cheap and disposable wearable sensors to make single use measurements, primarily in the area of biomarker detection. Herein we report the ability to make cheap (0.22 USD/sensor), disposable, wearable sensors by stitching conductive gold coated threads into fabrics. These threads are easily functionalised with thiolate self-assembled monolayers which can be designed for the detection of a broad range of different biomarkers. This all textile sensing platform is ideally suited to be scaled up and has the added advantage of being stretchable with insignificant effect on the electrochemistry of the devices. As a proof of principle, the devices have been functionalised with a continuous glucose sensing system which was able to detect glucose in human sweat across the clinically relevant range (0.1–0.6 mM). The sensors have a sensitivity of 126 ± 14 nA/mM of glucose and a limit of detection of 301 ± 2 nM. This makes them ideally suited for biomarker detection in point-of-care sensing applications.

1. Introduction

The field of wearable diagnostics has been growing in recent years (Bandodkar et al., 2019; Brothers et al., 2019; Chung et al., 2019; Gao et al., 2016; Lee et al., 2018; Matzeu et al., 2015). The ability to incorporate sensing technology into wearable devices to detect specific body movements, heart rate and body temperature has obvious benefits for the medical and sportswear industries; where products that fulfil this need have already been commercialized using conventional electronics (Germer et al., 2013; Xu et al., 2019). Notably, the success of the Apple watch and Fitbit® prove that there is a consumer demand for wearable sensing devices. To date however, most of these devices are rigid, brittle and expensive; so need to be incorporated into wearable watches or jewellery. Furthermore, they are unable to detect clinically relevant biomarkers. Whilst there have been some advances in the field of soft and flexible electronics for wearable sensing applications (Jeerapan and Poorahong, 2020), they still lack the breathability and ease of integration that a complete textile diagnostic sensing platform would offer (Keren et al., 2016; Munje et al., 2017). Textile based diagnostics have the advantage of not only being flexible, breathable and wearable; but can be easily incorporated into existing clothing manufacturing processes and can be produced on an industrial scale using existing technologies and infrastructure, which makes them cheap and scalable (Choudhary et al., 2015; Lund et al., 2018; Nilghaz et al., 2013; Oberg Mansson et al., 2020). As such, they can be used to realise disposable and single use wearable sensing modalities, which are prohibited by the high cost of smart watches and rings. Examples of disposable textile biosensing applications include, but are not limited to, testing for urinary tract infections in diapers (Reches et al., 2010) or infection in bandages (Derakhshandeh et al., 2018). Another useful application of textile sensors is in the field of glucose detection. Current technology requires diabetics to take regular blood samples to obtain blood glucose measurements using a glucometer. This is both invasive and gives a periodic sampling profile. It would be preferable to have a non-invasive continuous sensing platform capable of detecting glucose in the patients' sweat; since blood glucose levels and sweat glucose levels have been found to correlate (Gao et al., 2016; Lee et al., 2018; Moyer et al., 2012). Textiles offer the perfect platform for such devices as they can be

* Corresponding author.
** Corresponding author.
E-mail addresses: piper2@kth.se (A. Piper), mahiar@kth.se (M.M. Hamedi).

https://doi.org/10.1016/j.bios.2021.113604
Received 8 July 2021; Received in revised form 25 August 2021; Accepted 28 August 2021
Available online 1 September 2021

integrated into clothing and mass manufacturing processes; and naturally come into good contact with the patients' body and sweat. Such devices also have potential uses in the sportswear industry (Lee et al., 2017; Munje et al., 2017).

Much has been done on stress and movement sensors in the field of electrochemical textile sensors. However, non-invasive biomarker detection in excreted bodily fluids such as sweat (Katchman et al., 2018), urine (Liao et al., 2006), tears (Willcox, 2019), faeces (Pang et al., 2014), blood (Piper et al., 2018; Tsimikas et al., 2006) and milk (Alsaweed et al., 2015; Murphy et al., 2016) using electrochemical textile based biosensors is not widely reported. The current state of the art in flexible wearable sensors is primarily focussed on flexible polymer substrates with sensing elements integrated onto them (Jeerapan and Poorahong, 2020). These devices lack the breathability and ease of incorporation that an all textile sensor would offer, often needing adhesives to stick the patches onto the skin (Jeerapan and Poorahong, 2020). Alternatively screen printing electronics directly onto fabrics has been employed by Jeerapan et al., (2016), although this method would also reduce the breathability of the fabric at the sensor area. The current state of the art using conductive threads mostly involve the dip coating of threads with carbon pastes (Liu and Lillehoj, 2017) or elaborate methods of Au nanowire spin coating and electrodeposition of Au (Zhao et al., 2019); neither of which have been established as commercially viable. In the initial trails of this paper dip coated threads were tested but were found to crack and/or wick slowly towards the connection through the paste or inner cavities of a dip coated multifilament, leading to temporal instability of the signal and device failure over time.

Here we report for the first time the ability to stitch and functionalise a fully functioning electrochemical system into fabrics to create a cheap, disposable, stretchable and functional diagnostic platform, using commercially available Au plasma coated threads. In the devices reported here, the connection points of the threads can be quickly and easily separated from the electrode working area and any wicking to the connections is blocked. To validate the platform, it has been functionalised to make a label free continuous glucose sensor capable of detecting glucose in human sweat across a clinically relevant range. This involved functionalising the Au thread working electrodes with a thiolate self-assembled monolayer (SAM) compromising a glucose oxidase enzyme and a redox tagged thiol (6-Ferrocenylhexanethiol) which could be used to electrochemically regenerate the enzyme *in situ* and achieve a truly continuous glucose monitoring system by detecting the H_2O_2 produced by the enzymatic oxidation of glucose. Thiolate SAMs are perhaps the most widely used method of electrochemical sensor fabrication, to the best of the authors knowledge this is the first all textile device that can be functionalised with SAMs. This allows for their rapid integration with established SAM based biosensing methods to sense a broad range of biomarkers.

2. Experimental

2.1. Thread measurements in solution

Au multifilament thread (Swicofil AG, Switzerland) was taken as arrived and cut into short fragments. Nail varnish (Revlon, Sweden) was painted in the middle of each fragment and then left to dry for 1h. the threads were then cut to length so that one side of the nail varnish was 3 cm long. This was dipped into a solution of 5 mM potassium ferricyanide (III) (Sigma-Aldrich, Sweden) in 1x phosphate buffered saline (PBS, made from a 1x PBS tablet and 500 mL of Merck Millipore MilliQ Ultrapure water, 18.2 MΩ cm^{-1}). The other end of the threads were connected to an Autolab PGSTAT128N potentiostat (Metrohm, Sweden) to be used as working electrodes vs a commercial Ag/AgCl reference electrode (6 mm wide and 78 mm long with a single ceramic junction, VWR, Sweden) and Pt coil counter electrode (0.5 mm diameter, approximate total surface area of 4.7 cm^2). Cyclic voltammograms were recorded at a scan rate of 20 mVs-1 between −0.2 V and +0.4 V vs the $Ag/AgCl_2$ reference electrode.

The SEM of the Au threads provided in figure S1 was obtained on a Hitachi TM-1000 Tabletop SEM (Hitachi, Sweden).

2.2. Stitched device fabrication

Devices were stitched according to the following novel fabrication process. First, strips of Ripstop (Nooteboom textiles, Sweden) and the blended knit (96% cotton, 4% lycra; Nooteboom textiles, Sweden) were sewn together using a "Brother Innovis F480" (Brothers, Sweden) with cotton multifilament top and bobbin threads. The same Au multifilament used in 2.1. was lockstitched into these fabric strips using the same sewing machine with the Au multifilament as the bobbin thread and a polyamide (nylon) monofilament (Milcraft, UK) as the top thread. This was done in the pre-programmed mode "1–10" to get a zigzag pattern with the tension set to 4.0 units and the target width of the pattern being 1.0 mm and the distance between stitches being 2.0 mm. The working electrodes were stitched 3 cm long on the blended knit with ample length on the Ripstop to allow for a connection to the potentiostat. The pseudo-reference electrode was stitched using the same settings as the working electrode but was made only 1 cm long on the blended knit, again with enough length on the Ripstop to allow for potentiostat connection. The counter electrode was stitched to the same length as the working electrode but backstitched and then forward stitched again in the blended knit, so that three times the length of thread on the blended knit fabric in the working electrode was used in the counter electrode, 9 cm total. Again, enough length was added to the Ripstop to allow for connection to the potentiostat. After stitching a blob of nail varnish was generously applied on top of the Au threads on the Ripstop fabric close to the blended knit and allowed to dry, to prevent wicking along the Au multifilament threads to the connections. It is important when doing this step to make sure that the nail varnish permeates and fills the capillaries between the individual filaments of the thread. A schematic representation of the fabrication procedure has been provided in Fig. 1 and a photograph of a typical final device with all the component parts labelled has been provided in Fig. 3A.

2.3. Electrochemical characterisation of stitched devices

The stitched devices were connected to a potentiostat by crocodile clips on the Ripstop material. Aliquots (100 μL) of either 1x PBS (10 mM) or artificial sweat (VWR, Sweden) with or without (as specified in the data) 5 mM potassium ferricyanide (III) were pipetted onto the blended cotton knit. This would be left for 30s to allow the solution to completely wet all of the electrodes before measurements were started. Cyclic voltammograms were recorded between −0.3 V and +0.3 V vs the Au pseudo reference electrode and Au counter electrode at a scan rate of 20 mV/s. In order to test the flexibility of the devices they were stretched to 1.5 times their resting length and pinned into place on a polystyrene lid for the measurements to be taken see Fig. 4. The tension was removed and the measurement repeated. The stretching and relaxing was repeated 10 times.

To test the stretchability and wearability of the device, it was stitched into a wristband that could be worn by a volunteer (Fig. 4H and I). The human participant provided their informed written consent to wear the device and be a part of this study.

2.4. Glucose sensor fabrication

Devices were made as in section 2.2, however, only the working electrodes (not the counter and pseudo reference) were initially stitched. This strip of 8 working electrodes was functionalised by leaving in a dark fridge at 4 °C overnight in 10 mL of ethanol (96% Sigma-Aldrich, Sweden) with 4 mM 6-Ferrocenylhexanethiol and 5 mM 6-mercaptohexanoic acid (both from Sigma Aldrich, Sweden). These were then taken out and thoroughly rinsed first with ethanol and then 1x PBS to remove

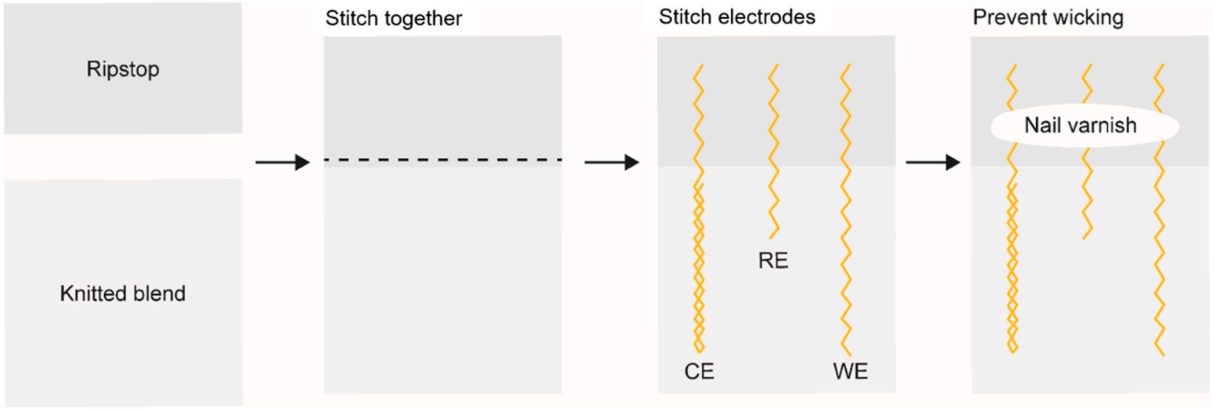

Fig. 1. Schematic representation of how stitched devices were fabricated prior to electrochemical characterisation.

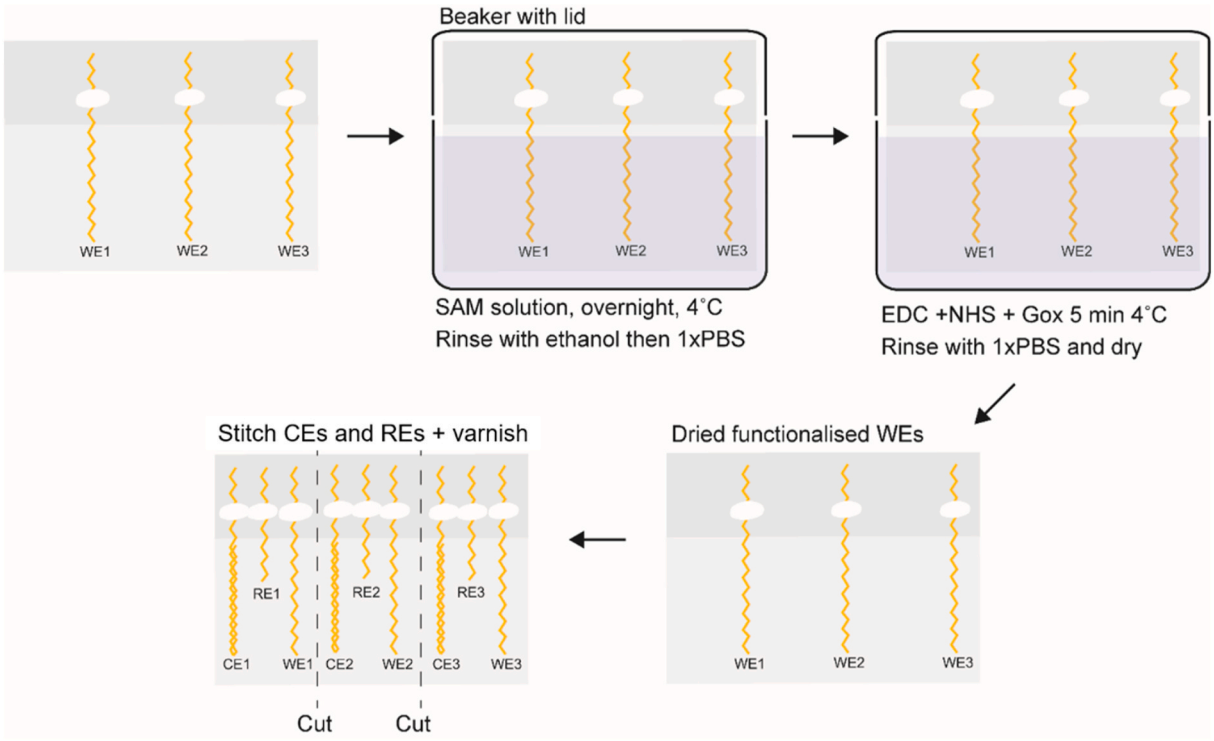

Fig. 2. Schematic representation of how multiple devices could be fabricated simultaneously and the working electrodes functionalised with thiolate self-assembled monolayers without functionalising the counter and reference electrodes.

physisorbed thiol from the devices. These were then placed in 25 mL of 4 mM 1-Ethyl-3-(3-dimethylaminopropyl)carbodiimide (EDC, Sigma Aldrich, Sweden), 1 mM N-hydroxysuccinimide (NHS, Sigma-Aldrich, Sweden) and 1 mg/mL glucose oxidase from *Aspergillus niger* (GOx, Sigma Aldrich, Sweden); for 25 min at 4 °C. These were then rinsed with 1x PBS before being allowed to dry in the dark. After drying the counter and reference electrodes could be stitched into the devices. A schematic showing how the functionalised devices are made is provided in Fig. 2. The devices were found to still be functional after storing for 5 days under N_2 in the dark at 4 °C.

2.5. Glucose sensor assay

The functional devices from section 2.4. were allowed to warm to room temperature before being connected via crocodile clips on the Ripstop section of the devices to the potentiostat. Cyclic voltammetry was performed consecutively in solutions of artificial human sweat (VWR, Sweden) and artificial human sweat spiked with 0.01 mM, 0.1 mM, 0.5 mM, 1 mM, 10 mM and 100 mM D-glucose (Sigma-Aldrich, Sweden). The artificial human sweat contains 19 amino acids, urea, lactic acid, ammonium chloride, NaCl and glacial acetic acid. As the devices contain no formal reference electrodes, a Au thread is being used as an un-calibrated quasi-reference electrode. As the potential of the reference electrode is not fixed, slight changes in the system such as temperature, buffer composition and contamination may cause slight deviations in the measured potentials in this system. At no point in this work do we analyse or try to interpret the potentials or potential shifts on these devices. The voltage window over which the CVs were performed was selected to incorporate the ferrocene redox peaks and H_2O_2 oxidation peak without reaching the solvent limits, whilst allowing for any changes in the pseudo-reference electrode potential. A voltage window of −0.3 V to +0.6 V vs a Au pseudo reference electrode and Au counter electrode at a scan rate of 20 mV/s was found to work best.

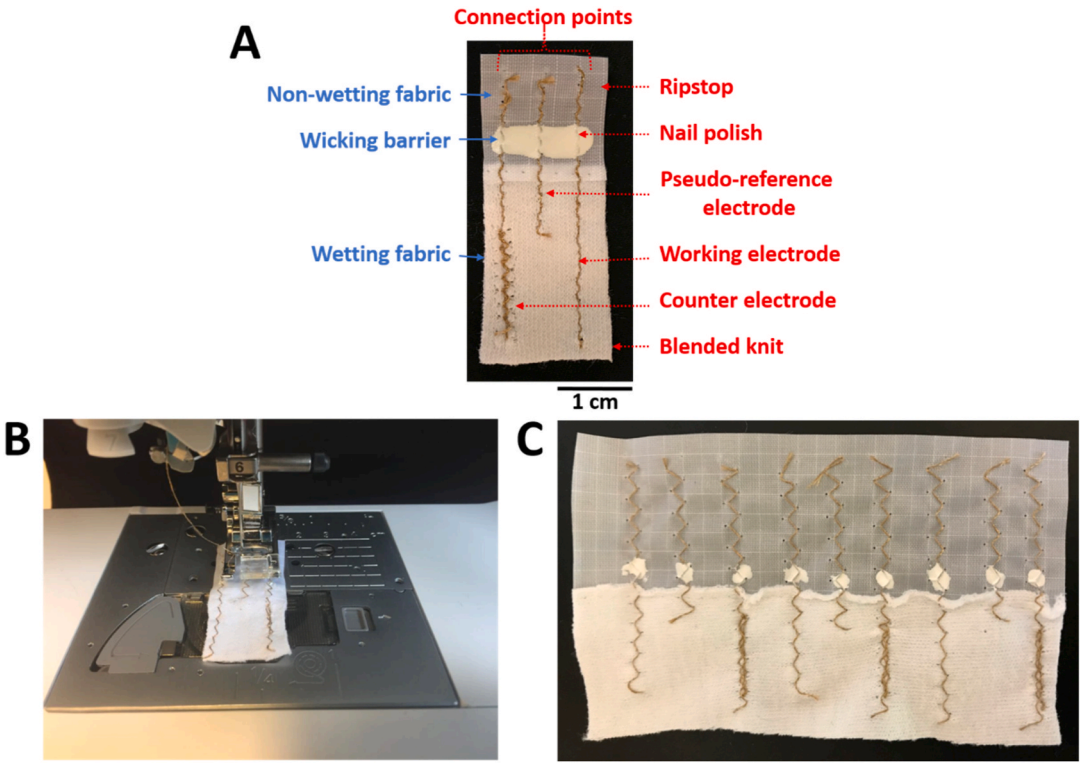

Fig. 3. Labelled photographs of the stitched sensing devices. Showing a single completed device (A), how the devices are stitched in a sewing machine (B) and how multiple devices could be manufactured simultaneously (C).

3. Results and discussion

3.1. Device design and fabrication

The devices could be lock stitched directly into the fabrics tested using a sewing machine with a nylon top thread and the Au multifilament as the bobbin thread. The Au coated multifilament threads are commercially available plasma coated PET single filaments (triangular in structure with a base width of 20 μm, see figure S1) that have been wound together to make a multifilament of 78 individual filaments. The basic electrochemistry of these threads in a wearable woven structure have been previously reported (Öberg Månsson et al.). One of the main advantages of these devices over established Au electrochemical biosensing platforms is that the Au threads required no pre-cleaning and have been used as received throughout this manuscript. This has obvious time and labour saving advantages for both sensor development and device scale up. The sewing machine allows for a variety of patterns to be stitched as well as control over the tension and spacing between the stitches. Each of these parameters needed to be optimised for the fabrics into which they were being stitched. For example, if the tension is too high when sewing into an elastic fabric, the fabric can deform.

Since the devices were stitched with a sewing machine and required no prior processing of any of the materials, they could be made in under 1 min and the design and shape easily iterated. In this manuscript the devices were stitched into Au/Au/Au three electrode systems with Au working electrodes 3 cm long, Au pseudo-reference electrodes 1 cm long and a counter electrode the same length as the working electrode but back and forward stitched three times so that a total of 9 cm of thread was used on the blended knit portion of the devices. In these devices there are two fabrics; a "Ripstop" 100% polyamide weave and a bleached blended knit of 96% cotton and 4% lycra. The blended knit is stretchable and extremely wetting, whereas the Ripstop is tough, non-wetting and hydrophobic. These are quickly and easily sewn together in long strips onto which multiple devices can be fabricated, see Fig. 3C. The purpose of the Ripstop is to create a zone into which the connections can be stitched where they will not get wet and short the system. The blended knit is stretchable and wetting so is an ideal fabric into which the functional parts of the device are stitched. There is no reason to believe that any fabric that retains liquid would not perform the same function. Since the multifilament Au threads wick solutions by micro capillary forces, a small amount of nail polish was painted onto the threads, to prevent wicking up to the connections, see Fig. 3A. The efficacy of the nail varnish barriers was tested by wetting the devices with food colouring and looking for evidence of the food colouring up the Au threads with and without nail polish, see Fig. 4F and G and S3. Nail varnish has previously been shown to be suitable for use in electrochemical biosensors and poses no threat to the wearer or the electrochemical system (de Lima et al., 2021). The distances between the working, counter and reference electrodes was chosen to be as small as possible, in order to minimise the total amount of base fabrics used to keep costs down. However, if the devices were stitched too closely to one another then any fraying of the thread filaments result in contact between the electrodes and short the system.

The costs for each of the materials are provided in Table 1. Given the dimensions of the devices, each prototype costs approximately 0.22 USD to make in house. Note that the cost of functionalisation is not factored into these calculations. This is purely the cost of the materials to make the device which can hypothetically be functionalised for a variety of different biomarkers. The cost per glucose sensing device in this study was calculated as 2.30 USD, using the cost of materials and exchange rates at the time of writing. The functionalisation was not optimised for cost and could be reduced further by bulk purchasing of the chemicals required. Given that these devices are so cheap and easy to produce they can be treated as disposable. By incorporating buttons or velcro into the devices they can easily and cheaply be integrated into existing textiles such as clothing; alternatively, they can be directly sewn into disposable, wearable devices such as shown in Fig. 4H and I.

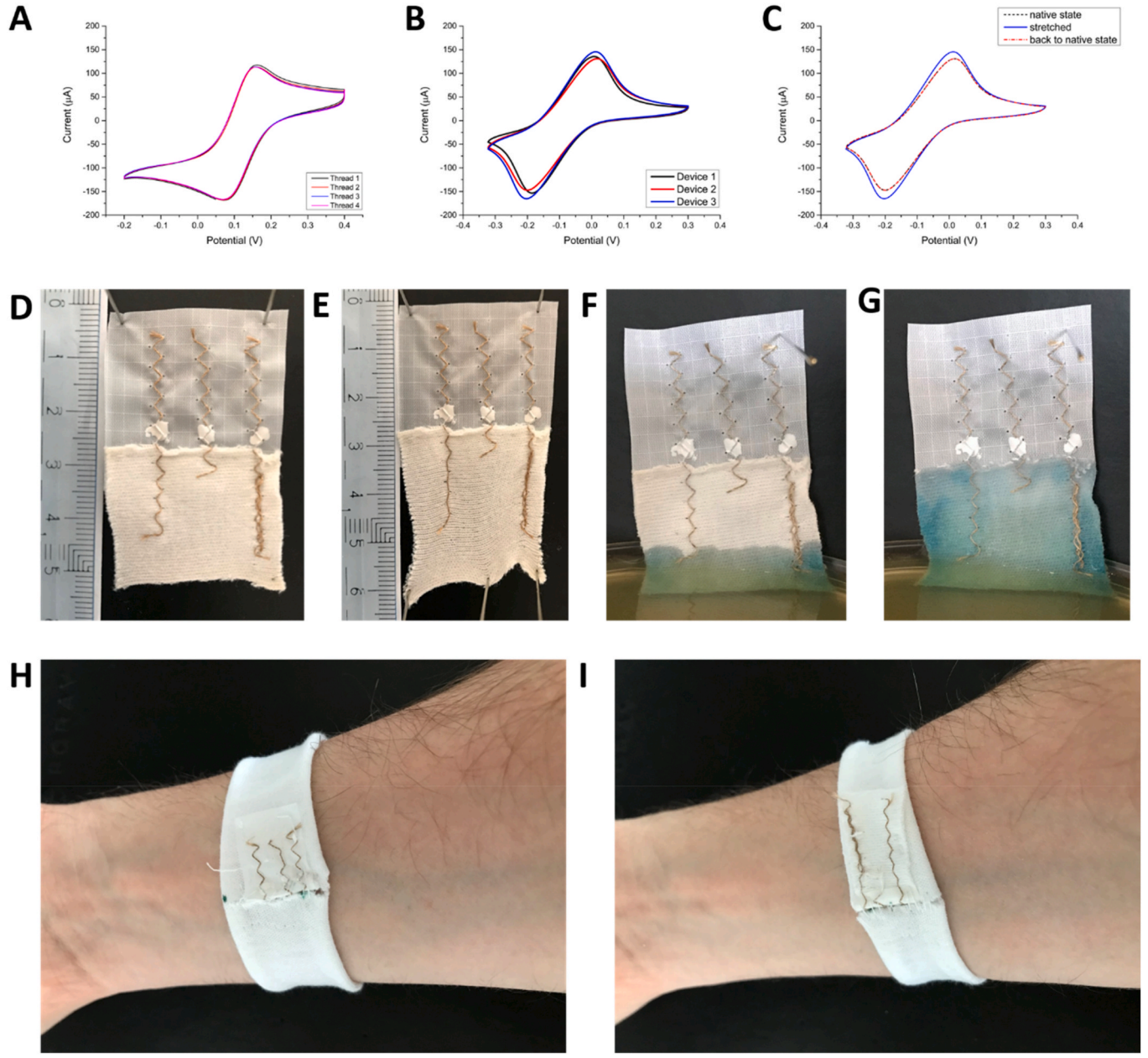

Fig. 4. (A) Cyclic voltammogramms of four separate cuts of Au thread measured in a solution of 1x PBS and 5 mM potassium ferricyanide (III), recorded vs a commercial Pt coil counter electrode and Ag/AgCl reference electrode at 20 mVs^{-1}; see fig S2 for a photograph of the set up. (B) Overlayed cyclic voltammograms of three separate stitched devices wet with 100 μL of 5 mM potassium ferricyanide (III) in 1x PBS, showing the reproducibility between devices. (C) Cyclic voltammograms of a single device when at rest, stretched to 150% and then back to being at rest. The cyclic voltammetry in (B) and (C) were recorded at 20 mVs^{-1} in an aqueous solution of 5 mM potassium ferricyanide (III) in 1x PBS *vs* the in-built Au pseudo-reference electrode. (D) Photograph of a device in the native, resting, state. (E) the same device shown in (D) stretched to 150% of the resting length. (F) and (G) show a device placed in potassium ferricyanide (III) to display how the liquid wicks up the stretchable, wetting fabric but not up the Ripstop or past the nail varnish up to the connections. (H) an exemplary wristband showing how the devices can be incorporated into a wearable device showing the top of the device where connections to a potentiostat can be made and (I) the same device shown in (H) turned inside out to show the part of the device that comes into direct contact with the skin.

3.2. Electrochemical characterisation of the devices

It is of interest and importance to understand any differences between the electrochemical behaviour of the threads when in solution and when stitched into the textile devices. The electrochemistry of the devices was characterised using potassium ferricyanide (III) in 1x PBS by cyclic voltammetry (CVs). The devices could not be analysed in sulfuric acid as it dissolved the base fabrics. The voltammograms of the Au threads in solution and stitched into the final devices have been provided in Fig. 4A and B respectively. Firstly, we can see that there is good reproducibility between the threads in solution and the stitched devices. Also the shapes of the CVs of the stitched devices indicate that they are under a similar diffusional regime to the threads in solution. This is suggestive of good wetting of all the electrodes and efficient mass transport within the chosen knitted blend fabric. To further establish this, the diffusion coefficient of ferricyanide (III) in each system could be calculated using the Randles'-Sevcik equation, Eqn. (1) (Xu, 2021):

$$i_l = 0.4463nFAc\left(\frac{nF\nu D}{RT}\right)^{\frac{1}{2}} \quad \text{(Eq 1)}$$

Table 1
Price of each component of the prototype stitched device and total cost per device. By buying each component in bulk the associated costs could be reduced further.

Material	Cost (USD)	Amount used per device	Cost/device (USD)
Ripstop	0.46/m^2	2.25 cm^2	0.0001
96% cotton 4% lycra blended knit	1.68/m^2	4.5 cm^2	0.0008
Multifilament Au thread	0.59/m	12 cm	0.0708
Nail varnish	3/mL	50 μL	0.1500
Cost per device			**0.2217**

Where i_l is the limiting current, n is the number of electrons being transferred, F is Faradays constant, *A* is the area of the electrode (taken as the geometric area based on a cylinder with the same dimensions as the thread, 3 cm long and 200 μm in diameter, 0.188 cm^2), c is the surface concentration of the redox agent (assumed to be the same as the bulk concentration, 5 mM), ν is the scan rate, D is the diffusion coefficient of the redox agent, R is the universal gas constant and T is the temperature. From the data in Fig. 4A and B the diffusion coefficients for ferricyanide (III) were found to be $6.79 \times 10^{-6} \pm 0.24 \times 10^{-6}$ cm^2 s^{-1} for the thread in solution and $9.92 \times 10^{-6} \pm 0.97 \times 10^{-6}$ cm^2 s^{-1} in the stitched devices. The slight variation between these values are believed to be the result of experimental error and that the diffusion of redox agent to in the textile devices is the same as that for in solution; and both are in agreement with literature values for the diffusion coefficient of ferricyanide and ferrocyanide in PBS. (Harned and Hudson, 1951; Konopka and McDuffie, 2002; Piper, 2017) At the very least mass transport is equally efficient in both systems and not in any way impeded by the fabric.

These findings suggest that any electrochemical analysis of the threads in solution will also hold for when stitched in these fabric devices, allowing the stitched devices to be analysed by established electrochemical theory. This is a key finding as it allows the electrochemical analysis of these devices using theories established on electrodes in solution.

3.3. Device flexibility

In most wearable applications the devices will be subjected to stretching, it is therefore beneficial for a wearable device to give a steady response with different degrees of stretching. In order to achieve this, in a textile device the threads can be stitched in a zigzag pattern that allows them to be stretched without damaging the device, see Fig. 4E. It was found that stitching in a zigzag pattern with a tension of 4.0 units, a target stitch width of 1 mm and the distance between stitches of 2 mm worked best for these devices. These settings were optimised for the fabrics used here and would need to be further optimised for different base fabrics. It is satisfying that the electrochemical response of the stitched devices in the native state and after elongating to 1.5 times the length gave nearly identical responses, see Fig. 4C and E. There is a slight increase in the peak redox currents (from +131 μA to +145 μA, and −147 μA to −165 μA) most probably due to the stretching of the device changing the twist of the thread and therefore slightly change the exposed electrode surface area. It is encouraging that the change in peak current is the same within error as the variation between separate devices, Fig. 4B, where the peak currents are $+138 \pm 8$ μA and -155 ± 10 μA for the oxidative and reductive peaks respectively. In multiplexed devices any stretching will not cause as significant a change as the inherent device to device variation. The peak potentials were unchanged by stretching the devices, Fig. 4C. Whilst the stability of the signal during a 150% elongation is impressive, it is hypothetically possible to design devices that can stretch further. The elasticity of the fabric substrate is what determines the elasticity of these devices and there is no reason to believe that a more elastic substrate would not be able to stretch further. It is also encouraging that when the tension was removed the electrochemical signal went back to what it was in the native state, Fig. 4C. These devices were fully stretched and relaxed 10 times over the course of a day without any change in electrochemical response, the data in Fig. 4C is after the 10th stretch and the initial native, non-stretched device. As the data all overlays so closely only these CVs have been included. There was some worry that the nail varnish may suffer some damage during the elasticity measurements. However, the portion of the threads on the Ripstop fabric remain unmoved during these experiments due to the inelastic nature of the Ripstop fabric, see Fig. 4E. As such the nail varnish was undamaged during these tests. Nail varnish was used to prevent wicking up the conductive Au threads to the connection points in these experiments because of it is inexpensive, widely available, inherently wearable and has previously been shown to be suitable for use in electrochemical systems (de Lima et al., 2021).

The wearable nature of the devices has been shown in Fig. 4H and I where a device has been sewn into a flexible arm band that can be slid on and off the wrist over the hand. It is also hypothetically possible to integrate Velcro or buttons into these devices so that they can be added to existing textiles such as clothing to be used as a disposable patch rather than a disposable item of clothing such as the wristband shown here. These devices were incorporated into wristbands since previous literature has shown that there is a steady supply of sweat with a composition that is close to the average whole body sweat composition on the forearms, and the skin temperature is similar to the lab temperatures in which the devices were tested (20–30 °C). (Baker et al., 2018; Leonov and Vullers, 2007).

3.4. Proof of concept glucose sensor

To validate the diagnostic utility of the platform it was functionalised to make a glucose sensor. This was done by forming a mixed SAM of 6-ferrocenylhexanethiol (FHT) and 6-mercaptohexan-1-ol (MHA) in a 1:1 stoichiometric ratio on the working electrode. Devices were made with only the working electrodes stitched and these were incubated in the afore mentioned SAM mixture, in ethanol, overnight at 4 °C in the dark. The next day these Au/FHT/MHA electrodes were functionalised by coupling glucose oxidase (GOx) to the MHA in the SAM through carbodiimide coupling. After this, the Au/FHT/MHA/MHA-GOx electrodes were allowed to dry under ambient conditions before the counter and reference electrodes were stitched into each of the devices. A schematic showing the chemistry of the sensors has been provided in Fig. 5A. The glucose oxidase bound to the electrode surface reacts with β-D-glucose and O_2 to generate D-glucono-1,5-lactone and H_2O_2; the latter of which is electrochemically active and produces an oxidation peak at +450 mV *vs* the Au pseudo reference electrode in this system. The size of this hydrogen peroxide peak correlates to the amount of glucose in the solution in a 1:1 stoichiometric ratio. The FHT was included because it can regenerate the glucose oxidase to achieve continuous glucose monitoring (Dicks et al., 1993).

Fig. 5B shows the voltammetric response of a single device in artificial sweat spiked with 0.01, 0.1, 0.5 1, 10 and 100 mM glucose consecutively. A clear increase in capacitance as well as the peak assigned to hydrogen peroxide at +450 mV *vs* the pseudo reference electrode can be observed. Replicates of this experiment have been included in figure S4 and a calibration curve showing the mean current and standard deviation (σ) from three repeats has been provided in Fig. 5C. The current is a direct measurement of the amount of H_2O_2 produced by the glucose oxidase, given that the GOx from *Aspergillus niger* has previously been shown to have a Michaelis constant (K_M) = 1–4 mM when immobilised on an electrode (Cho and Bailey, 1978), over the concentration range investigated here, a log-linear response is expected. The log-linearity of the devices is advantageous as it means the sensor is more sensitive over the clinically relevant range than a purely linear response. The response shows that the sensors have a dynamic

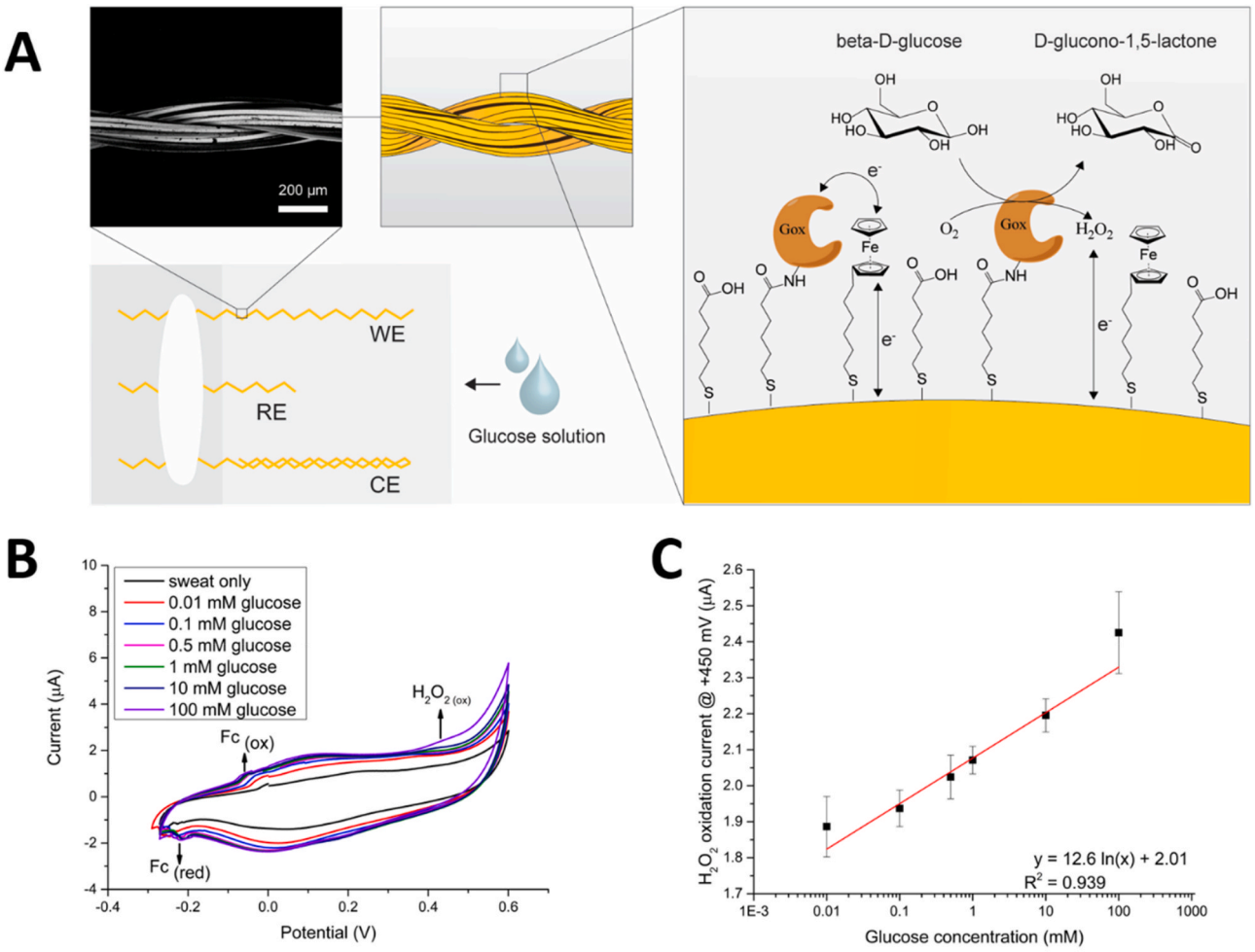

Fig. 5. (A) Schematic representation of one of the devices with an inset SEM of an unstitched Au thread and a schematic (not to scale) of the chemistry of the glucose detection taking place on the functionalised Au/FHT/MHA/MHA-GOx filaments. Showing the regeneration of the glucose oxidase by the ferrocene hexanethiol and the reaction of glucose oxidase with glucose to produce hydrogen peroxide which can be detected electrochemically. (B) Overlaid cyclic voltammograms of artificial human sweat spiked with increasing concentrations of glucose, with the ferrocene and hydrogen peroxide peaks labelled. (C) Log-dose response curve showing the increase in the hydrogen peroxide peak current as a function of glucose concentration. Three repeats were done to determine the standard deviation given by the error bars.

range across the concentration range (0.01 mM–100 mM), which is well in excess of the clinically relevant range for glucose in sweat (0.1 mM–0.6 mM) (Bandodkar et al., 2019; Brasier and Eckstein, 2019; Chung et al., 2019; Moyer et al., 2012; Oberg Mansson et al., 2020). The sensors have a sensitivity of 126 ± 14 nA/mM of glucose and a limit of detection (LOD) = 301 ± 2 nM. Based on the geometric area of the working electrodes, the sensitivity per unit area is 88 ± 10 nA mM^{-1} cm^{-2}. Typically other devices have limits of detection in the µM range, whereas the limit of detection of these devices is 301 ± 2 nM; likewise we report sensitivities of 88 ± 10 nA mM^{-1} cm^{-2} which is superior those found elsewhere which are in the range of µA mM^{-1} cm^{-2} (Jeerapan et al., 2016; Zhao et al., 2019). The performance of these sensors is comparable to that of ELISA and Western blot tests, therefore this platform could potentially be used to develop point-of-care devices to replace such tests. These are all prototype devices made by hand, on a small scale, using a basic commercial sewing machine. It is reasonable to assume that a larger scale process with automated manufacturing techniques might improve the reproducibility of the devices and allow for them to be miniaturized which would reduce material costs further.

By virtue of the fact that the measurements were performed in artificial human sweat which contains 19 amino acids urea, lactic acid, ammonium chloride, NaCl and glacial acetic acid. The selectivity of the sensor is considered more than sufficient for glucose detection in sweat.

There was some concern that the volume of sweat produced by the body would not wet the devices sufficiently for them to operate. In this study, 25 µL aliquots of artificial sweat were used. It should be noted that the volume of sweat produced per minute varies on different parts of the body and from person to person. The average sweat rate on the forearm is 0.2 mg/cm^2/min under normal physiological conditions (Buono et al., 2008). Given that the density of sweat is the same as water, since sweat is water based, the volume of sweat produced on the forearm is therefore 0.2 mL/cm^2/min. Far in excess of the amounts that we have tested here which were 0.005 mL/cm^2 (the devices are 4.5 cm^2 and 25 µL aliquots were used). Once the absorbent part of the devices was wet it typically took >15 min to dry out. Therefore, the devices will stay sufficiently wet to perform measurements under normal sweating conditions.

To assay each device across the clinically relevant concentration range would typically take 4–6 h, over which timescale the devices would give a steady response. It is therefore possible to conclude that the functionalised devices were able to continuously measure different concentrations of glucose in artificial human sweat over a 4–6 h period. These measurements were only stopped because the assays had been completed. The devices did fail however if, after being assayed, they were allowed to dry overnight and were then re-wet and used the next

day.

4. Conclusions and future work

The efficacy and suitability of plasma coated Au conductive threads stitched into fabrics to make stitched electrochemical sensing platforms has been established. This all textile sensing platform using Au plasma coated multifilament threads stitched into Ripstop and an elastic blended knit could be stretched by 150% without impairment of the observed electrochemical response. The ability to functionalise the stitched devices and diagnostic utility of the platform have been established by functionalising to create a glucose sensor capable of detecting glucose in human sweat over a clinically relevant range. The low cost of these devices (0.22c per device) makes them inherently disposable. Therefore, this sensing platform can be utilised for low cost wearable sensing operations to which current, more expensive, wearable technology such as smart watches are not suited. In this work have for the first time developed a simple and scalable method of stitched diagnostic device fabrication and functionalisation with thiolate self-assembled monolayers. The simplicity of this method makes it inherently more scalable and practical than other reported methodologies of wearable sensor fabrication and the method allows for the easy incorporation of existing SAM based biosensors which are widely reported in the literature. Likewise, the commercial availability on an industrial scale of all the device components evidences their scalability.

The performance of these reported devices has been exhibited by the development and optimisation of a continuous sweat based glucose sensor on the textile devices that exceeds the performance of other textile biosensors reported in the literature. Future work will include trying to integrate the sensors with a wearable potentiostat. Such a potentiostat needs to be small, robust, light and waterproof. Once developed it would allow for the analysis of these devices worn on different parts of the body and during different exercises which would affect the sweat composition and device temperature, both of which could theoretically affect the performance of the devices. Given the performance of the devices, further work should also include functionalising them to detect a variety of biomarkers in sensing media to which textile platforms are well suited; such as sweat biomarkers, urine biomarkers in diapers and blood based biomarkers in bandages.

Author contributions

A.P., M.H., and I.Ö.M. conceived the original ideas. A.P. led the project, performed the experiments, and data analysis, and wrote the manuscript. I.Ö.M. helped with the device construction and the choice of materials, electrochemical characterisation and SEM measurements. R. L. helped develop the devices for portable potentiostat integration. S.K. did work on Au thread analysis and development.

CRediT authorship contribution statement

Andrew Piper: conceived the original ideas, led the project, performed the experiments, Formal analysis, and data analysis, and wrote the manuscript. **Ingrid Öberg Månsson:** conceived the original ideas, helped with the device construction and the choice of materials, electrochemical characterisation and SEM measurements. **Shirin Khaliliazar:** Formal analysis, did work on Au thread analysis and development. **Roman Landin:** helped develop the devices for portable potentiostat integration.

Declaration of competing interest

The authors declare that they have no known competing financial interests or personal relationships that could have appeared to influence the work reported in this paper.

Acknowledgements

The authors thank Contifibre for providing Coolmax yarn, and Swicofil for guidance and discussions on the metal plasma coated yarns. The authors also acknowledge the Knut and Alice Wallenberg Foundation and the European Research Council (Grant 715268) for funding.

Appendix A. Supplementary data

Supplementary data to this article can be found online at https://doi.org/10.1016/j.bios.2021.113604.

References

Alsaweed, M., Hepworth, A.R., Lefevre, C., Hartmann, P.E., Geddes, D.T., Hassiotou, F., 2015. J. Cell. Biochem. 116 (10), 2397–2407.
Baker, L.B., Ungaro, C.T., Sopeña, B.C., Nuccio, R.P., Reimel, A.J., Carter, J.M., Stofan, J. R., Barnes, K.A., 2018. J. Appl. Physiol. 124 (5), 1304–1318.
Bandodkar, A.J., Jeang, W.J., Ghaffari, R., Rogers, J.A., 2019. In: Bohn, P.W., Pemberton, J.E. (Eds.), Annual Review of Analytical Chemistry, vol. 12, pp. 1–22.
Brasier, N., Eckstein, J., 2019. Digit Biomark 3 (3), 155–165.
Brothers, M.C., DeBrosse, M., Grigsby, C.C., Naik, R.R., Hussain, S.M., Heikenfeld, J., Kim, S.S., 2019. Accounts Chem. Res. 52 (2), 297–306.
Buono, M.J., Claros, R., DeBoer, T., Wong, J., 2008. J. Appl. Physiol. 105 (4), 1044–1048.
Cho, Y.K., Bailey, J.E., 1978. Biotechnol. Bioeng. 20 (10), 1651–1665.
Choudhary, T., Rajamanickam, G.P., Dendukuri, D., 2015. Lab Chip 15 (9), 2064–2072.
Chung, M., Fortunato, G., Radacsi, N., 2019. J. R. Soc. Interface 16 (159), 20190217-20190217.
de Lima, L.F., Ferreira, A.L., Maciel, C.C., Ferreira, M., de Araujo, W.R., 2021. Talanta 227, 122200.
Derakhshandeh, H., Kashaf, S.S., Aghabaglou, F., Ghanavati, I.O., Tamayol, A., 2018. Trends Biotechnol. 36 (12), 1259–1274.
Dicks, J.M., Cardosi, M.F., Turner, A.P.F., Karube, I., 1993. Electroanalysis 5 (1), 1–9.
Gao, W., Emaminejad, S., Nyein, H.Y.Y., Challa, S., Chen, K.V., Peck, A., Fahad, H.M., Ota, H., Shiraki, H., Kiriya, D., Lien, D.H., Brooks, G.A., Davis, R.W., Javey, A., 2016. Nature 529 (7587), 509–+.
Germer, S., Cherkouk, C., Rebohle, L., Helm, M., Skorupa, W.,2013; Proc. SPIE 8767, Integrated Photonics: Materials, Devices, and Applications II, 876710 (22 May 2013); doi:10.1117/12.2017275.
Harned, H.S., Hudson, R.M., 1951. J. Am. Chem. Soc. 73 (11), 5083–5084.
Jeerapan, I., Poorahong, S., 2020. J. Electrochem. Soc. 167 (3), 037573.
Jeerapan, I., Sempionatto, J.R., Pavinatto, A., You, J.-M., Wang, J., 2016. J Mater Chem A Mater 4 (47), 18342–18353.
Katchman, B.A., Zhu, M.L., Christen, J.B., Anderson, K.S., 2018. Proteonomics Clin. Appl. 12 (6).
Keren, D.M., Efrati, A., Maita, F., Maiolo, L., Minoti, A., Pecora, A., Fortunato, G., Zajac, M., Shacham-Diamand, Y., 2016. IEEE ASME Trans. Mechatron. https://doi.org/10.1109/ICSEE.2016.7806127.
Konopka, S.J., McDuffie, B., 2002. Anal. Chem. 42 (14), 1741–1746.
Lee, H., Hong, Y.J., Baik, S., Hyeon, T., Kim, D.H., 2018. Adv. Healthc. Mater. 7 (8).
Lee, H., Song, C., Hong, Y.S., Kim, M.S., Cho, H.R., Kang, T., Shin, K., Choi, S.H., Hyeon, T., Kim, D.H., 2017. Science Advances 3 (3).
Leonov, V., Vullers, R., 2007. In: Proceedings - 5th European Conference on Thermoelectrics, vol. 47.
Liao, J.C., Mastali, M., Gau, V., Suchard, M.A., Moller, A.K., Bruckner, D.A., Babbitt, J.T., Li, Y., Gornbein, J., Landaw, E.M., McCabe, E.R.B., Churchill, B.M., Haake, D.A., 2006. J. Clin. Microbiol. 44 (2), 561–570.
Liu, X., Lillehoj, P.B., 2017. Biosens. Bioelectron. 98, 189–194.
Lund, A., Darabi, S., Hultmark, S., Ryan, J.D., Andersson, B., Ström, A., Müller, C., 2018. Advanced Materials Technologies 3 (12), 1800251.
Matzeu, G., Florea, L., Diamond, D., 2015. Sensor. Actuator. B Chem. 211, 403–418.
Moyer, J., Wilson, D., Finkelshtein, I., Wong, B., Potts, R., 2012. Diabetes Technol. Therapeut. 14 (5), 398–402.
Munje, R.D., Muthukumar, S., Prasad, S., 2017. Sensor. Actuator. B Chem. 238, 482–490.
Murphy, J., Sherman, M.E., Browne, E.P., Caballero, A.I., Punska, E.C., Pfeiffer, R.M., Yang, H.P., Lee, M., Yang, H., Gierach, G.L., Arcaro, K.F., 2016. Breast Canc. Res. Treat. 157 (1), 13–22.
Nilghaz, A., Ballerini, D.R., Shen, W., 2013. Biomicrofluidics 7 (5).
Oberg Mansson, I., Piper, A., Hamedi, M.M., 2020. Macromol. Biosci. 20 (11), e2000150.
Pang, T., Leach, S., Katz, T., Day, A., Ooi, C., 2014. Frontiers in Pediatrics 2 (6).
Piper, A., 2017. Chemistry. University of Edinburgh.
Piper, A., Alston, B., Adams, D., Mount, A.R., 2018. Faraday Discussions.
Reches, M., Mirica, K.A., Dasgupta, R., Dickey, M.D., Butte, M.J., Whitesides, G.M., 2010. ACS Appl. Mater. Interfaces 2 (6), 1722–1728.
Tsimikas, S., Willerson, J.T., Ridker, P.M., 2006. J. Am. Coll. Cardiol. 47 (8_Suppl. ment), C19–C31.
Willcox, M.D., 2019. Clin. Exp. Optom. 102 (4), 350–363.

Xu, K., 2021. J. Micromech. Microeng. 31 (5), 054001.
Xu, K., Chen, Y., Okhai, T.A., Snyman, L.W., 2019. Opt. Mater. Express 9 (10), 3985–3997.
Zhao, Y., Zhai, Q., Dong, D., An, T., Gong, S., Shi, Q., Cheng, W., 2019. Anal. Chem. 91 (10), 6569–6576.